The effect of Er doping on the multiferroics of $Ho_{1-x}Er_xMnO_3$

2008 J. Phys.: Condens. Matter 20 035211

(http://iopscience.iop.org/0953-8984/20/3/035211)

J. Phys.: Condens. Matter **20** (2008) 035211 (5pp) doi:10.1088/0953-8984/20/03/035211

The effect of Er doping on the multiferroics of $Ho_{1-x}Er_xMnO_3$

H D Zhou[1], **R Vasic, J Lu, J S Brooks and C R Wiebe**

Department of Physics, Florida State University, Tallahassee, FL 32306-3016, USA
and
National High Magnetic Field Laboratory, Florida State University, Tallahassee, FL 32306-4005, USA

E-mail: zhou@magnet.fsu.edu

Received 27 July 2007, in final form 19 October 2007
Published 17 December 2007
Online at stacks.iop.org/JPhysCM/20/035211

Abstract

The magnetic phase diagram of single-crystalline $Ho_{1-x}Er_xMnO_3$ below T_N (antiferromagnetic transition temperature) is determined by measuring the magnetic susceptibility (χ), specific heat (C_P), and dielectric constant (ε). Er doping enhances the $P6_3cm$ magnetic phase above T_{SR} (spin-reorientation temperature) and therefore decreases T_{SR}. Er doping also reduces the $P6_3cm$ phase below T_2 (rare-earth element ordering temperature). The change of entropy around T_{SR} with Er doping shows that the Er^{3+}-ion spin is ordering at T_{SR}. This ordering helps to narrow the $P6_3cm$ to $P6_3cm$ magnetic phase transition and enhance the coupling between the Ho^{3+}/Er^{3+} and Mn^{3+} magnetic sublattices, which is shown by the dielectric constant measurements.

(Some figures in this article are in colour only in the electronic version)

1. Introduction

The $RMnO_3$ compounds with hexagonal structure (R from Ho to Lu and Y) have attracted considerable recent attention because of the coupling between ferrielectricity and antiferromagnetic order [1–9]. The high temperature hexagonal $P6_3/mmc$ structure contains close-packed planes of Mn^{3+} ions in bipyramidal oxygen coordination separated by planes of R^{3+} ions. A cooperative rotation of the bipyramidal axis from the c axis below a temperature T_t loses the mirror planes perpendicular to the c axis and changes the symmetry to $P6_3cm$. These rotations also induce a ferrielectric displacement of the R^{3+} ions along the c axis below a Curie temperature $T_C < T_t$ without a further change in crystal symmetry [1, 10, 11]. The dominant spin–spin interactions between Mn^{3+} ions within the close-packed basal planes are geometrically frustrated (GF), which lowers the antiferromagnetic ordering temperature T_N of the Mn^{3+} ions to a $T_N \ll T_C$. With different rare-earth element on the A-site, $RMnO_3$ shows different magnetic symmetry below T_N. $HoMnO_3$, $YMnO_3$, and $ErMnO_3$ are three examples of systems with very different ground states. For $HoMnO_3$, below $T_N \approx 70$ K, the magnetic symmetry changes from $P6_3cm$ to $P6_3cm$ at $T_{SR} = 33$ or 40 K [11, 12] with a 90° rotation of the Mn spins. The symmetry then changes to $P6_3cm$ at $T_2 \approx 5$ K with another 90° rotation of the Mn spins, which is accompanied by a antiferromagnetic ordering of the Ho^{3+}-ion spins orientated along the c axis [1, 13]. For $YMnO_3$ and $ErMnO_3$, the magnetic symmetries are $P6_3cm$ and $P6_3cm$, respectively, below $T_N \approx 70$ K [14]. There is a ferrimagnetic ordering of Er^{3+}-ion spins below 5 K [15]. Several open questions remain, however, considering the effect of Er or Y doping upon the $HoMnO_3$ ground states.

Recently we reported the magnetic phase diagram of (HoY) MnO_3 which shows that Y doping increases T_{SR} and decreases T_2 [16]. Here we further clarify the effect of Er doing on the magnetic phase diagram and multiferroicity of (HoEr)MnO_3.

2. Experiment

Single crystals of $Ho_{1-x}Er_xMnO_3$ ($0 \leqslant x \leqslant 0.4$) were grown by the traveling-solvent floating-zone (TSFZ) technique. All samples were single phase with the hexagonal $P6_3cm$ structure via powder x-ray diffraction. The XRD patterns were

[1] Author to whom any correspondence should be addressed.

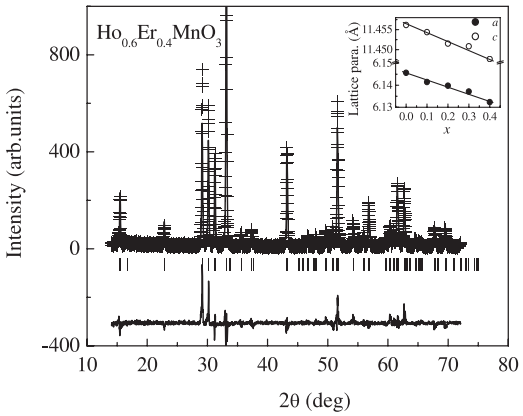

Figure 1. Room temperature XRD pattern for $Ho_{0.6}Y_{0.4}MnO_3$ (plus marks). The solid curve is the best fit from the Rietveld refinement using FullProf. The vertical marks indicate the position of the Bragg peaks, and the bottom curve shows the difference between the observed and calculated intensities. Inset: variation of lattice parameters a and c with x for $Ho_{1-x}Er_xMnO_3$.

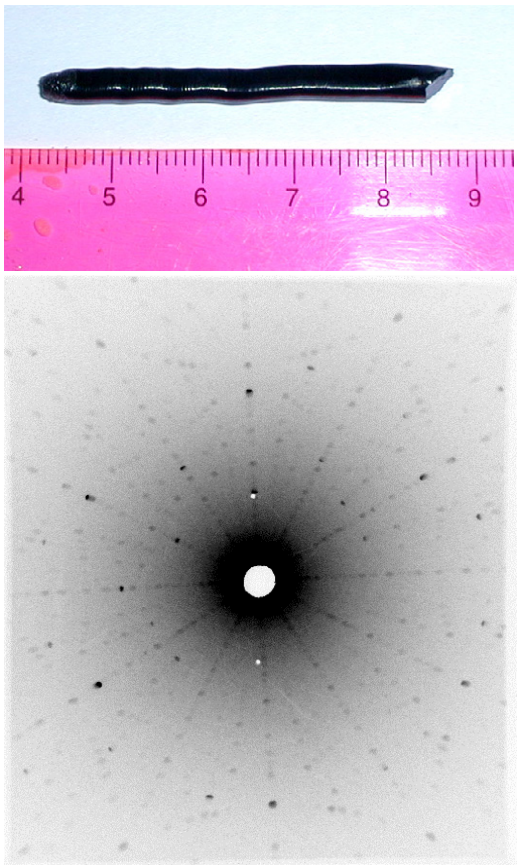

Figure 2. Single crystal of $HoMnO_3$ and its x-ray Laue pattern along the c axis.

refined by using program FullProf with typical $R_p \approx 9\%$, $R_{wp} \approx 12\%$ and $\chi^2 \approx 2$. With increasing x, the lattice parameters a and c both decrease linearly, figure 1. X-ray Laue diffraction was used to orient the crystal, figure 2. The magnetic susceptibility measurements were made with a Quantum Design dc superconducting interference device

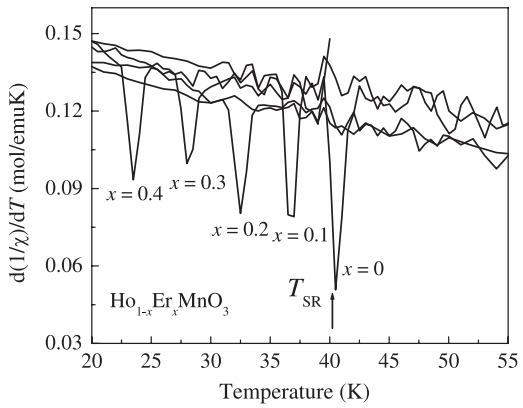

Figure 3. Temperature dependences of $d(1/\chi)/dT$ with $20\ K < T < 55\ K$ for $Ho_{1-x}Er_xMnO_3$.

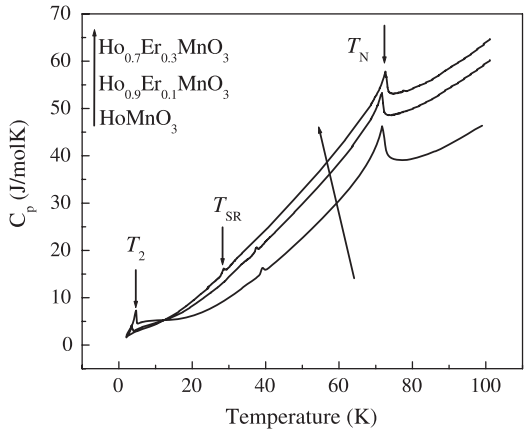

Figure 4. Temperature dependences of specific heat C_p for selected $Ho_{1-x}Er_xMnO_3$.

(SQUID) magnetometer with an applied field of 100 Oe along the c axis; the measurements were made after cooling in zero field (ZFC). The specific heat measurements were performed on a PPMS (Physical Property Measurement System, Quantum Design) at temperatures from 2 to 100 K. A standard ac capacitance bridge method was used to measure the real (capacitative—C) and loss (dissipative—D) signals at 100 kHz with parallel plate silver electrodes normal to the c axis and with magnetic fields along the c direction or in the ab plane.

3. Results

Figure 3 shows the temperature dependences of $d(1/\chi)/dT$ for $Ho_{1-x}Er_xMnO_3$ over the temperature range $20\ K < T < 55\ K$. The derivatives show peaks at T_{SR}, which is 40 K for $HoMnO_3$. With increasing x, T_{SR} decreases.

The specific heat data of $Ho_{1-x}Er_xMnO_3$ shows three anomalies: (i) a λ-type anomaly at T_N, figure 4; (ii) a narrow peak around T_{SR}, figure 5(a), which is plotted as C_{SR}/T (C_{SR}/T is obtained by subtracting a linear background fit from C_P/T in a small temperature range near T_{SR}); and (iii) a sharp peak at T_S, figure 5(b). With increasing x, (i) T_N remains around 70 K; (ii) the intensity of the peaks around T_{SR} and T_2, and also the values of T_{SR} and T_2 both decrease.

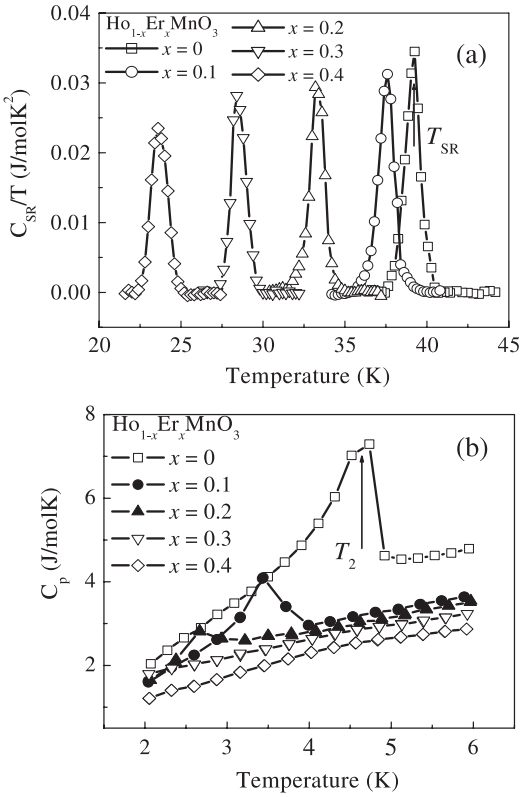

Figure 5. Temperature dependences of specific heat C_p around T_{SR} (a) and T_2 (b) for $Ho_{1-x}Er_xMnO_3$.

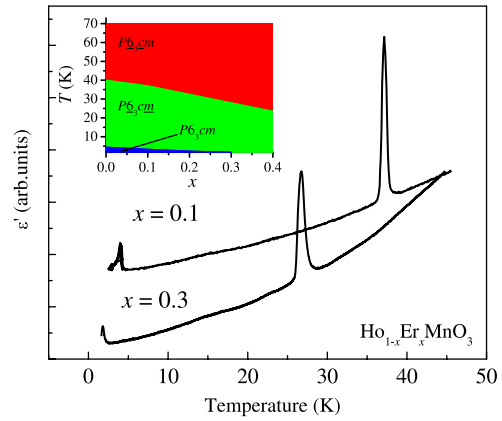

Figure 6. Temperature dependences of dielectric constant $\varepsilon Ho_{1-x}Er_xMnO_3$. Inset: the magnetic phase diagrams below 70 K for $Ho_{1-x}Er_xMnO_3$.

The dielectric constant data of $Ho_{1-x}Er_xMnO_3$, figure 6, shows sharp peaks around T_{SR} and T_2. The values of T_{SR} and T_2 obtained here are consistent with those obtained from susceptibility and specific heat measurements.

Figure 7 shows the temperature dependences of the dielectric constant (ε) with applied fields $H \parallel c$ and $H \parallel ab$ for $Ho_{0.9}Er_{0.1}MnO_3$. All data show the dielectric constant peaks around T_{SR} and T_2, and their magnetic field dependences. The measured value of the dielectric constant of $Ho_{0.9}Er_{0.1}MnO_3$ is approximately 12, which is smaller than that of pure $HoMnO_3$ ($\varepsilon = 16$). With $H \parallel c$, the ε peak broadens and evolves into

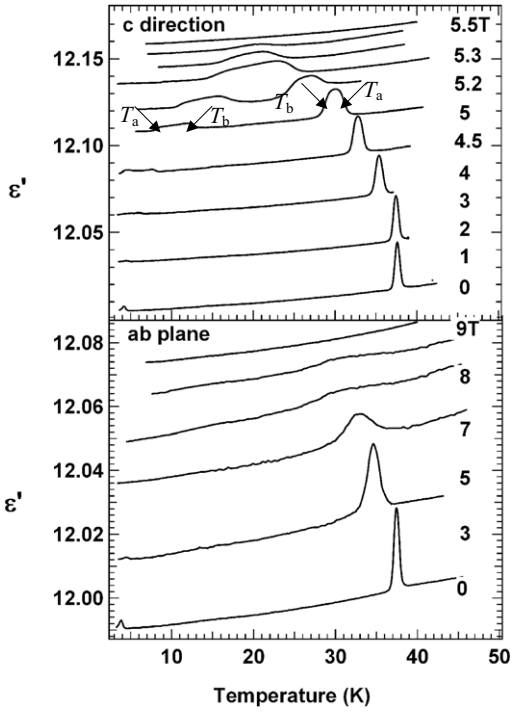

Figure 7. Temperature dependences of the real part of the dielectric constant for $Ho_{0.9}Er_{0.1}MnO_3$ at different magnetic fields with $H \parallel c$ (upper panel) and $H \parallel ab$ (lower panel). For $H = 0$, the curves are shifted upwards by arbitrary amounts.

a plateau-like structure with a increase at T_a and a drop at T_b; T_a and T_b are taken as the half-maxima positions on both sides of the plateau. At higher fields a second ε plateau develops at lower temperatures, with further increasing H the two plateaus merge into each other and final disappear. For $H \parallel a$, there is no second plateau. Both T_a and T_b show overall agreement with previous determinations of the $H \parallel c$ 're-entrant' phase diagram [4].

The magnetic field–temperature phase diagrams determined by T_a and T_b for $Ho_{0.9}Er_{0.1}MnO_3$ with $H \parallel c$ and $H \parallel ab$ were plotted in figure 8 and its inset, respectively. The diagram for $HoMnO_3$ is also included for comparison. T_a and T_b separate the novel phase from the $P6_3cm$ and $P6_3cm$ phases. So the difference between T_a and T_b or the full width at half-maxima of the dielectric constant peaks determines the widths of the transitions. With Er doping, two features are noteworthy from the phase diagram: (i) the width of the dielectric constant peak around T_{SR} becomes narrower; (ii) the re-entrant phase boundaries shrink in the temperature range, which means a lower T_{SR}, but expand along the applied field axis. The maximum field required to suppress T_{SR} is approximately 5 T, compared to the pure $HoMnO_3$ case where the maximum field is about 4 T.

4. Discussions

The magnetic phase diagram below 70 K for $Ho_{1-x}Er_xMnO_3$ determined by T_{SR} and T_2 is shown in figure 6 (inset). The magnetic phase of $ErMnO_3$ below 70 K is $P6_3cm$, so the Er doping favors the formation of the $P6_3cm$ magnetic phase below T_N. At the same time, T_{SR} is controlled by the magnetic

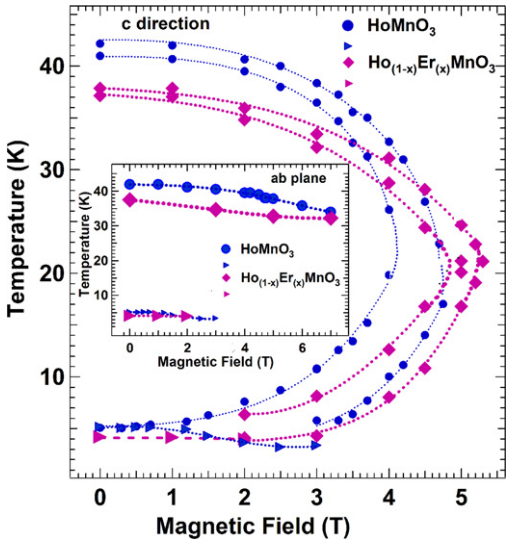

Figure 8. Magnetic field–temperature phase diagrams for $Ho_{0.9}Er_{0.1}MnO_3$ and $HoMnO_3$ with $H \parallel c$ and $H \parallel ab$ (Inset). Dashed lines are guides to the eye. The intermediate phase boundary widths correspond to the dielectric constant half-widths.

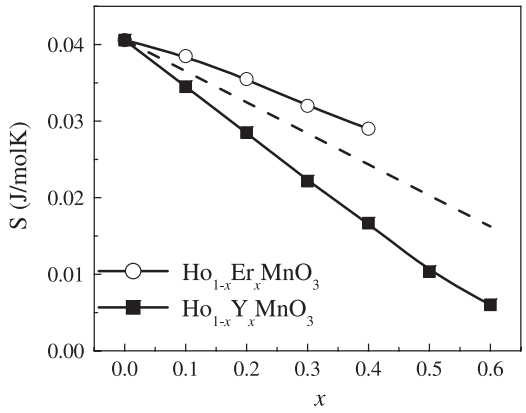

Figure 9. Variation with x of the calculated entropy around T_{SR} for $Ho_{1-x}Y_xMnO_3$ and $Ho_{1-x}Er_xMnO_3$. The lines are just guides for the eye.

phase transition between $P6_3\underline{cm}$ and $P\underline{6_3}c\underline{m}$, so with Er doping, T_{SR} decreases. Er doping also reduces the $P6_3cm$ phase, so T_2 decreases with increasing x. This effect may be from the competition between the antiferromagnetic ordering of Ho^{3+} spins and the ferrimagnetic ordering of Er^{3+} spins below 5 K. The effect of Er doping on T_{SR} of $HoMnO_3$ is the opposite to that of Y doping [16]. The completed magnetic phase diagrams of $Ho_{1-x}Er_xMnO_3$ and $Ho_{1-x}Y_xMnO_3$ show that the multiferroicity of $HoMnO_3$ is tunable by changing the volume fractions of the different magnetic phases below T_N.

The observed peak for the specific heat around T_{SR} of $HoMnO_3$ is due to the partial Ho^{3+} spin ordering, which has also been inferred from DC susceptibility and neutron scattering data [13, 17, 18]. The reorientation of the Mn spins is strictly confined in the ab plane. It cannot account for the entropy change at T_{SR}. Figure 9 shows the variation with x of the calculated entropy around T_{SR} for $Ho_{1-x}Er_xMnO_3$ and $Ho_{1-x}Y_xMnO_3$. The dashed line is the calculation of $S = S_0 * (1 - x)$, which represents the effect of simple non-magnetic ion doping on Ho^{3+} site; here x is the doping level. $S_0 = 0.04\ \mathrm{J\,mol^{-1}\,K^{-1}}$ is the entropy of $HoMnO_3$, which is consistent with the value obtained from single crystals grown by the flux method. With Y doping, the entropy change is below the dash line, which means that Y doping not only reduces the magnetic Ho^{3+} ions but also dilutes the Ho–O–Ho interactions to reduce the entropy associated with Ho^{3+} spin orderings. But with Er doping, the entropy change is above the dashed line, which means there must be some Er^{3+} ions are ordering around T_{SR}.

The origin of the dielectric constant peak aroundT_{SR} for $HoMnO_3$ is due to crossing the magnetic phase boundary between the $P6_3\underline{cm}$ to $P\underline{6_3}c\underline{m}$ symmetries, which is also coupled to the Ho^{3+} ion ordering [17]. The half-width of the dielectric constant peak represents the intermediate phase boundary width and the maximum field needed to suppress the T_{SR} represents the strength of the coupling between the Ho^{3+} and Mn^{3+} sublattices. Doping with Er^{3+} ions leads to a sharper phase transition (as seen through sharper dielectric constant anomalies, figure 7) and stronger coupling between the Ho^{3+}/Er^{3+} and Mn^{3+} sublattices (as demonstrated with the robustness of the ordered phase in applied fields compared to $HoMnO_3$, figure 8). These effects from Er doping could be the results of the extra Er^{3+} ion ordering around T_{SR}, which has been suggested by the specific heat measurements as discussed above. The stronger coupling between the Ho^{3+}/Er^{3+} and Mn^{3+} sublattices with lower T_{SR} for Er doping samples shows that T_{SR} is controlled by the magnetic phase transition of Mn^{3+} spins, but the dielectric constant behavior is related to the coupling between the Ho^{3+}/Er^{3+} and Mn^{3+} sublattices.

5. Conclusions

Based on the present studies of $Ho_{1-x}Er_xMnO_3$, it has been demonstrated that: (i) Er doping decreases T_{SR} by enhancing the $P6_3\underline{cm}$ magnetic phase above T_{SR}. Er doping also diminishes the $P6_3cm$ phase below T_2; (ii) the specific measurements show the ordering of Er^{3+} ion around T_{SR}; (iii) this extra ordering helps to narrow the magnetic phase transition at T_{SR} and enhance the coupling between the Ho^{3+}/Er^{3+} ion and Mn^{3+} ion sublattices.

Acknowledgments

This work is supported by a contractual agreement between the NSF and the State of Florida through NHMFL. A portion of this work was supported by NSF Cooperative Agreement No. DMR-0084173, by the State of Florida, and by the DOE. The authors would also like to acknowledge the support of Florida State University through the EIEG program.

References

[1] Van Aken B B, Palstra T T M, Filippetti A and Spaldin N A 2004 *Nat. Mater.* **3** 164
[2] Fiebig M, Fröhlich D, Kohn K, Leute St, Lottermoser Th, Pavlov V V and Pisarev R V 2000 *Phys. Rev. Lett.* **84** 5620

[3] Lee S, Pirogov A, Hoon H J, Park J G, Hoshikawa A and Kamiyama T 2005 *Phys. Rev.* B **71** 180413(R)
[4] Lorenz B, Litvinchuk A P, Gospodinov M M and Chu C W 2004 *Phys. Rev. Lett.* **92** 087204
[5] dela Cruz C R, Yen F, Lorenz B, Wang Y Q, Sun Y Y, Gospodinov M M and Chu C W 2005 *Phys. Rev.* B **71** 060407(R)
[6] Adem U, Nugroho A A, Meetsma A and Palstra T T 2007 *Phys. Rev.* B **75** 014108
[7] Vasic R, Zhou H D, Jobiliong E, Wiebe C R and Brooks J S 2007 *Phys. Rev.* B **75** 014436
[8] Laukhin V, Skumryev V, Martí X, Hrabovsky D, Sánchez F, Garciá-Cuenca M V, Ferrater C, Varela M, Lüders U, Bobo J F and Fontcuberta J 2006 *Phys. Rev. Lett.* **97** 227201
[9] Tachibana M, Yamazaki J, Kawaji H and Atake T 2005 *Phys. Rev.* B **72** 064434
[10] Coeuré P, Guinet P, Peuzin J C, Buisson G and Bertaut E F 1966 *Proc. Int. Meeting on Ferroelectricity* vol 1, ed V Dvorák, A Fousková and P Glogar, pp 332–40
[11] Zhou H D, Denyszyn J C and Goodenough J B 2005 *Phys. Rev.* B **72** 224401
[12] Yen F, dela Cruz C R, Lorenz B, Sun Y Y, Wang Y Q, Gospodinov M M and Chu C W 2005 *Phys. Rev.* B **71** 180407(R)
[13] Muñoz A, Alonso J A, Martínez-lope M J, Casáis M T, Martínez J L and Fernández-Díaz M T 2001 *Chem. Mater.* **13** 1497
[14] Fiebig M, Lottermoser T, Fröhlich D, Goitsev A V and Pisarev R V 2002 *Nature* **419** 818
[15] Fiebig M, Degenhardt C and Pisarev R V 2002 *Phys. Rev. Lett.* **88** 027203
[16] Zhou H D, Lu J, Vasic R, Vogt B W, Brooks J S and Wiebe C R 2007 *Phys. Rev.* B **75** 132406
[17] Lorenz B, Yen F, Gospodinov M M and Chu C W 2005 *Phys. Rev.* B **71** 014438
[18] Lonkai Th, Hohlwein D, Ihringer J and Prandl W 2002 *Appl. Phys.* A **74** 843